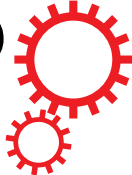


# SCIENTIFIC REPORTS



OPEN

## Electric and Magnetic Hotspots via Hollow InSb Microspheres for Enhanced Terahertz Spectroscopy

Mahdiyeh Sadrara & MirFaez Miri 

We study electric and magnetic hotspots in the gap between hollow InSb microspheres forming dimers and trimers. The outer radius, core volume fraction, distance, and temperature of the microspheres can be chosen to achieve field enhancement at a certain frequency corresponding to the transition between energy levels of a molecule placed in the gap. For example, utilizing 80  $\mu\text{m}$  radius spheres at a gap of 2  $\mu\text{m}$  held at a temperature of 295 K, allow electric field intensity enhancements of 10–2880 and magnetic field intensity enhancements of 3–61 in the frequency window 0.35–1.50 THz. The core volume fraction and the ambient temperature affect the enhancements, particularly in the frequency window 1.5–2 THz. Electric and magnetic hotspots are promising for THz absorption and circular dichroism spectroscopy.

In the past two decades, the generation and detection of coherent terahertz (THz) radiation have attracted much attention<sup>1,2</sup>. THz spectroscopy holds great promise for many applications in physics and chemistry<sup>3,4</sup>. The majority of studies exploit the Fourier transform spectroscopy and THz time-domain spectroscopy. In Fourier transform spectroscopy, the sample is illuminated with a broadband source. The sample is positioned in a Michelson interferometer and the path length of one of the arms of the interferometer is changed. The Fourier transform of the interference signal yields the absorption spectrum of the sample. In THz time-domain spectroscopy, these are the amplitude and phase of the electric field of THz pulses transmitted through the sample that determine its absorption and dispersion spectra.

THz spectroscopy has been used to study structure and dynamics of atoms and molecules. Many interesting results have been obtained, for instance: (i) Solute-induced changes in water's hydrogen bonding network near lactose are investigated. It is found that the hydration layer around lactose extends to  $\approx 5 \text{ \AA}$  from the surface corresponding to  $\approx 123$  water molecules beyond the first solvation shell<sup>5</sup>. (ii) Upon illumination by light, bacteriorhodopsin (BR) changes its conformation. It is observed that the photocycling time of the D96N mutant is about 1000 times that of the wild-type BR. The THz absorption of the mutant is smaller than that of the wild-type. This suggests that the mutant has lower conformational flexibility<sup>6</sup>. (iii) The low-frequency phonons of carbon nanotubes are directly observed<sup>7</sup>. (iv) The tunneling-inversion in methyl halides such as  $\text{CH}_3\text{Cl}$  is demonstrated<sup>8</sup>.

Recently, the interest in THz circular dichroism spectroscopy is growing<sup>9–11</sup>. Unlike the absorption, the circular dichroism (the differential absorption of right- and left-circularly polarized light) is sensitive to the molecular chirality. Based on the abundance of biological chiral molecules, it is proposed that THz circular dichroism spectroscopy will be of use in searching for extraterrestrial life<sup>9</sup>. However, THz circular dichroism signals are extremely weak. This issue needs to be addressed.

In the visible and near-infrared regions of the spectrum, the spectroscopy techniques have been augmented with the use of *electric hotspots*<sup>12–19</sup>. Metallic nanoparticles supporting surface plasmons, concentrate light in small subwavelength volumes. Enhanced local electric fields significantly increase the interaction of light with atoms and molecules. In other words, hotspots may help to overcome the sensitivity limitations of conventional spectroscopy methods. Plasmonic enhanced fluorescence<sup>15–17</sup>, surface Raman optical activity of chiral molecules<sup>18</sup>, and surface Raman scattering<sup>12</sup> are reported. Dielectric nanoparticles have recently gained attention due to the inherent ohmic losses of metallic nanoparticles which lead to heat perturbations on a nearby emitter<sup>20,21</sup>. Intense magnetic field in gaps separating dielectric nanoparticles are theoretically predicted<sup>22</sup> and experimentally observed<sup>23,24</sup>. *Magnetic hotspots* also enhance the interaction of light with atoms and molecules: The basic Hamiltonian describing the interaction of an electromagnetic field and a quantum emitter is  $H_{\text{int}} = -\mathbf{d} \cdot \mathbf{E} - \mathbf{m} \cdot \mathbf{B}$  where  $\mathbf{d}$  and  $\mathbf{m}$  denote the electric and magnetic dipole

Department of Physics, University of Tehran, P.O. Box 14395-547, Tehran, Iran. Correspondence and requests for materials should be addressed to M.M. (email: [mirfaez\\_miri@ut.ac.ir](mailto:mirfaez_miri@ut.ac.ir))

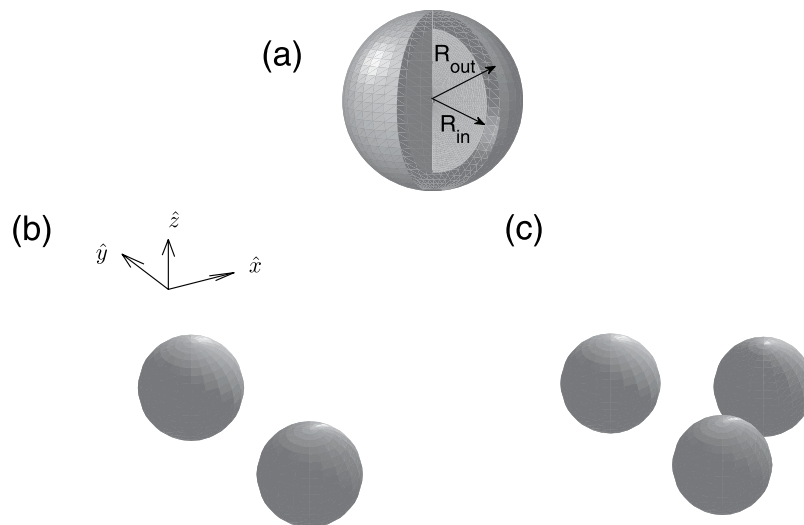


**Figure 1.** Schematic representation of (a) one, (b) two, and (c) three hollow InSb microspheres.

moments of the emitter, respectively. Indeed  $\text{Im}(\mathbf{d} \cdot \mathbf{m}) \neq 0$  is a requisite for exhibiting circular dichroism<sup>25</sup>. Dielectric nanoparticles allow substantial increase of the circular dichroism signal<sup>26,27</sup>. Electric and magnetic hotspots provided by dimers and trimers of solid<sup>28,29</sup> and hollow nanoparticles<sup>30</sup> may find application in single molecule experiments. Hotspots provided by disordered and fractal aggregates of nanoparticles are also studied<sup>31–35</sup>. In particular, it is shown that fractal clusters of hollow silicon nanoparticles provide both electric and magnetic hotspots. In the wavelength window 400–750 nm, electric field intensity enhancements of 10–400 and magnetic field intensity enhancements of 10–3790 are reported<sup>35</sup>.

Taking advantage of the field enhancement for the spectroscopic studies, is beginning to be explored in the THz region of the spectrum<sup>36–43</sup>. For example, Park *et al.* utilized field enhancement within a nanoslit (a nano-aperture on a thin metallic film) to detect nanograms of molecules such as 1,3,5-trinitroperhydro-1,3,5-triazine (RDX)<sup>38</sup>. Toma *et al.* showed that engineered arrays of rectangular nanoantennas coupled through narrow gaps allow THz spectroscopy of a monolayer of CdSe quantum dots<sup>40</sup>. These impressive successes invites one to add to the arsenal of methods of THz field enhancement. Not only methods to achieve large field enhancements, but also simple and cheap methods deserve attention.

Indium antimonide (InSb) whose plasma frequency is in the THz range, has been widely used as a THz material<sup>37,44–46</sup>. Here we study electric and magnetic hotspots in the gap between hollow InSb microspheres forming dimers and trimers (see Fig. 1). The outer radius, core volume fraction, distance, and temperature of the microspheres can be chosen to address the necessity of intensity enhancement at a certain frequency corresponding to transition between energy levels of a molecule placed in the gap. For example, utilizing 80  $\mu\text{m}$  radius spheres at a gap of 2  $\mu\text{m}$  held at a temperature of 295 K, allow electric field intensity enhancements of 10–2880 and magnetic field intensity enhancements of 3–61 in the frequency window 0.35–1.50 THz. Here the core volume fraction and the ambient temperature influence the intensity enhancements, particularly in the frequency window 1.5–2 THz. Electric and magnetic hotspots provided by InSb microspheres are promising for THz absorption and circular dichroism spectroscopy.

## Model

We consider dimers and trimers of hollow InSb microspheres (see Fig. 1). We characterize the  $\alpha$ th hollow microsphere by its position  $\mathbf{r}_\alpha$ , inner radius  $R_{\text{in}}$ , and outer radius  $R_{\text{out}}$ . We use  $f = (R_{\text{in}}/R_{\text{out}})^3$  to denote the core volume fraction. The permittivity of InSb can be well described by the Drude model<sup>47</sup>

$$\varepsilon(\omega, T) = \varepsilon_\infty - \frac{\omega_p^2(T)}{\omega^2 + i\omega\gamma(T)} \quad (1)$$

where  $\omega$ ,  $T$ ,  $\varepsilon_\infty$ ,  $\omega_p$ , and  $\gamma$  are angular frequency, ambient temperature, high-frequency permittivity, plasma frequency, and damping factor, respectively.  $\varepsilon_\infty = 15.75$ .  $\omega_p(T) = \sqrt{4\pi n_c(T)e^2/m^*}$ , where the intrinsic carrier density is<sup>48</sup>

$$n_c(T) = 5.76 \times 10^{14} T^{1.5} \exp\left(-\frac{0.129 \text{ eV}}{k_B T}\right) \text{ cm}^{-3} \quad (2)$$

$e$  is the charge of electron,  $m_e$  is the mass of electron,  $m^* = 0.015m_e$  is the effective mass, and  $k_B$  is the Boltzmann constant. In particular<sup>49</sup>

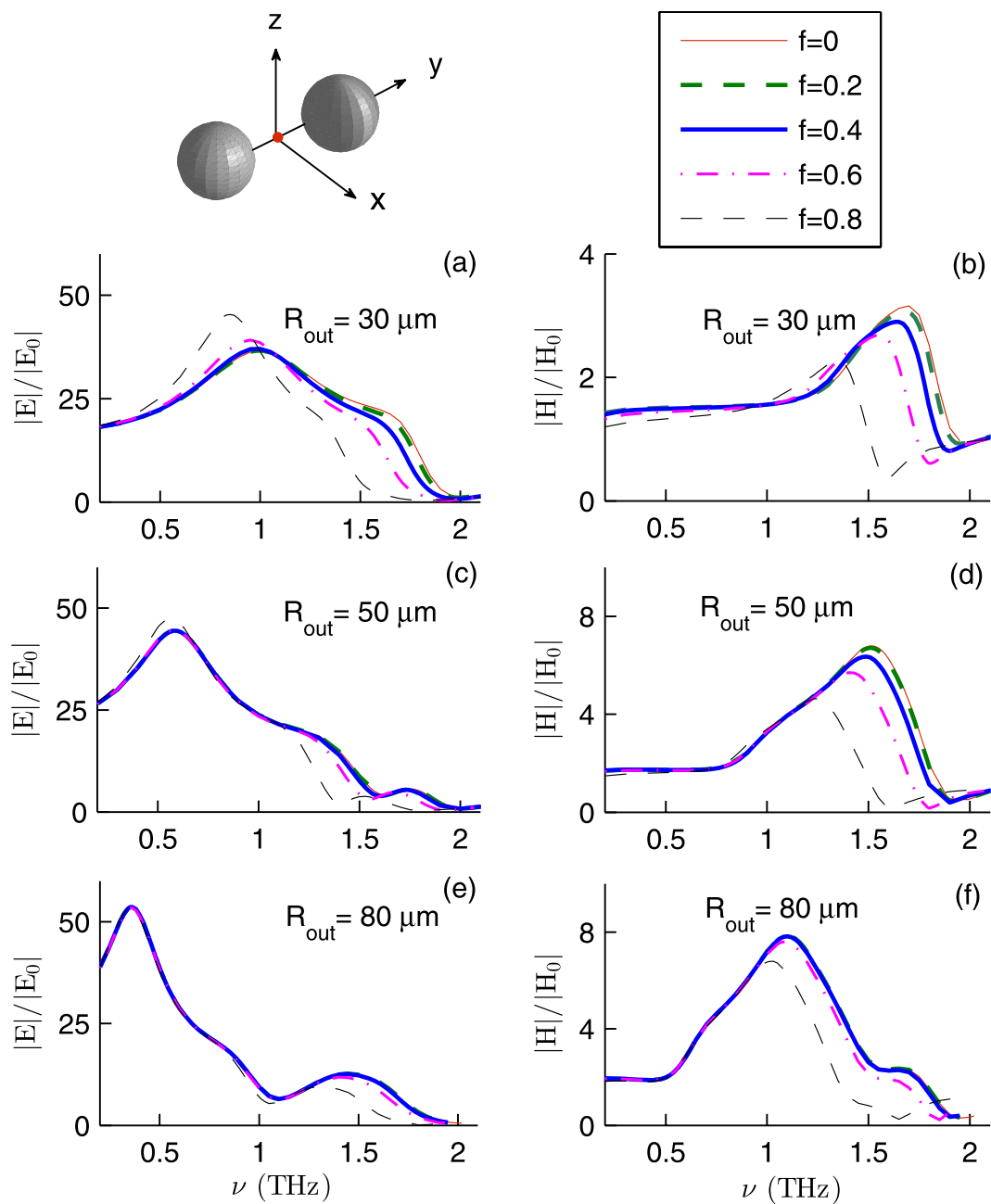


**Figure 2.** The field enhancement factors for InSb dimer as a function of the frequency  $\nu$  for various  $R_{out}$  and  $f$ . Here  $T = 295$  K,  $\mathbf{E}_i \parallel \hat{y}$ ,  $\mathbf{k}_i = -k\hat{z}$ , and the fields are calculated at the dimer center  $(\mathbf{r}_1 + \mathbf{r}_2)/2$ .

$$\begin{aligned} \left(\frac{\omega_p}{2\pi}, \frac{\gamma}{2\pi}\right) &= (8.0, 0.26) \text{ THz at } T = 295 \text{ K} \\ \left(\frac{\omega_p}{2\pi}, \frac{\gamma}{2\pi}\right) &= (9.0, 0.28) \text{ THz at } T = 310 \text{ K} \\ \left(\frac{\omega_p}{2\pi}, \frac{\gamma}{2\pi}\right) &= (9.9, 0.31) \text{ THz at } T = 325 \text{ K} \end{aligned} \tag{3}$$

We assume that the incident fields are

$$\begin{aligned} \mathbf{E}_i &= E_0 \hat{\mathbf{u}}_i e^{i\mathbf{k}_i \cdot \mathbf{r} - i\omega t} \\ \mathbf{H}_i &= H_0 \hat{\mathbf{k}}_i \times \hat{\mathbf{u}}_i e^{i\mathbf{k}_i \cdot \mathbf{r} - i\omega t} \end{aligned} \tag{4}$$

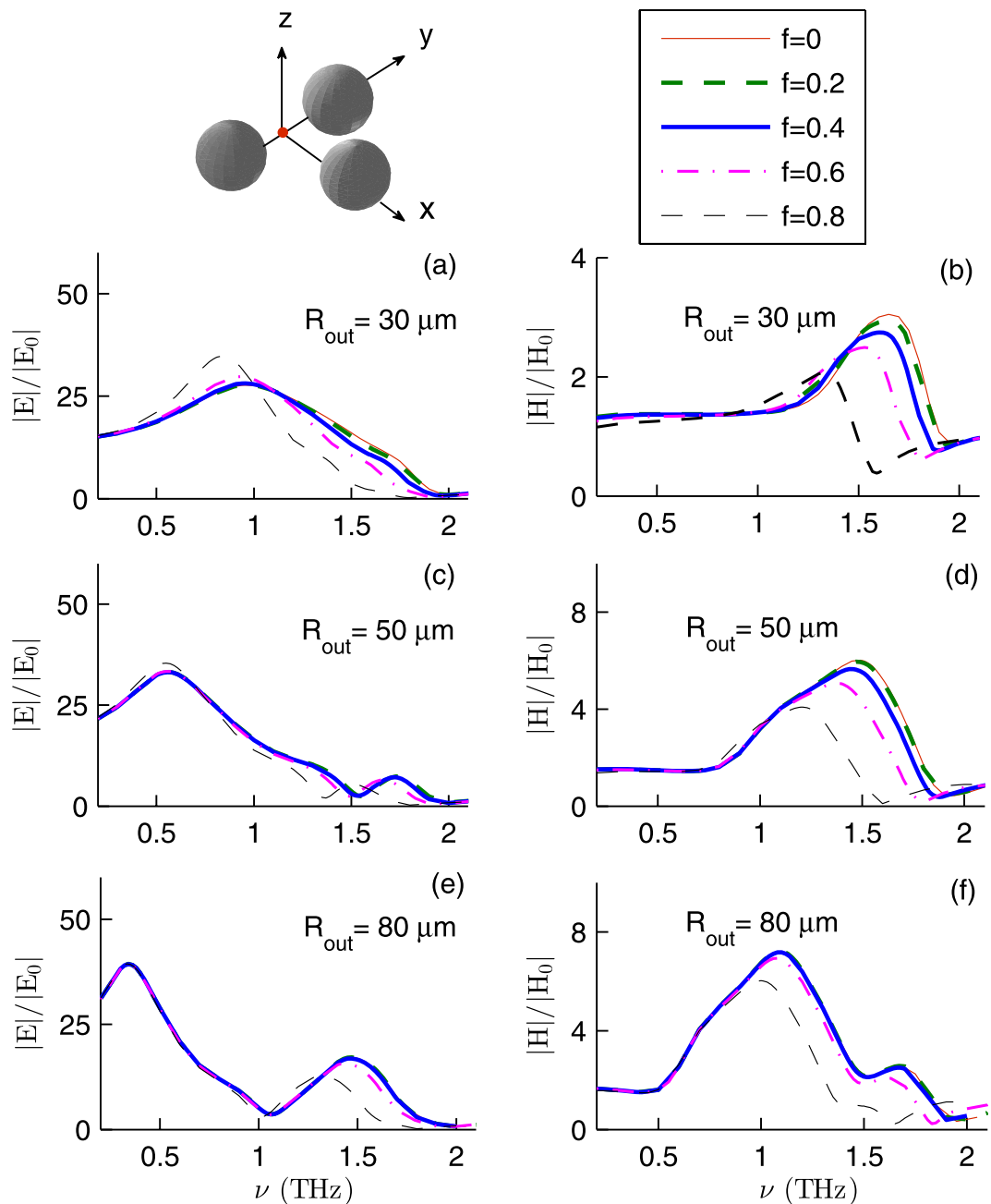


**Figure 3.** The field enhancement factors for InSb trimer as a function of  $\nu$  for various  $R_{\text{out}}$  and  $f$ . Here  $T = 295$  K,  $E_{\text{I}} \parallel \hat{y}$ ,  $\mathbf{k}_{\text{I}} = -k\hat{z}$ , and the fields are calculated at  $(\mathbf{r}_1 + \mathbf{r}_2)/2$ .

The amplitude  $E_0$ , polarization unit vector  $\hat{\mathbf{u}}_{\text{I}}$ , wave vector  $\mathbf{k}_{\text{I}}$ , and angular frequency  $\omega = 2\pi\nu$  characterize the incident wave.  $H_0 = E_0$ ,  $\hat{\mathbf{u}}_{\text{I}} \cdot \hat{\mathbf{k}}_{\text{I}} = 0$  and  $k = |\mathbf{k}_{\text{I}}| = \omega/c$ , where  $c$  is the velocity of light in vacuum. Following the theory developed in ref.<sup>30</sup>, we calculate the electromagnetic field distribution in the vicinity of the hollow microspheres. We use cgs units.

## Results and Discussion

**Field enhancement via InSb dimers and trimers.** We assume that two identical hollow InSb microspheres are at positions  $\mathbf{r}_1 = (0, R_{\text{out}} + d_p/2, h_p)$  and  $\mathbf{r}_2 = (0, -R_{\text{out}} - d_p/2, h_p)$ . We study the field enhancement factors  $|E/E_0|$  and  $|H/H_0|$ , where  $E$  and  $H$  denote the amplitudes of the total electric and magnetic fields at the observation point. The frequency  $\nu_E$  ( $\nu_H$ ) where the electric (magnetic) field enhancement factor gains its maximum, is of particular interest. We study InSb spheres of outer radius 30, 50 and 80  $\mu\text{m}$ . We assume that  $d_p = 2 \mu\text{m}$  and  $h_p = 1$  nm.

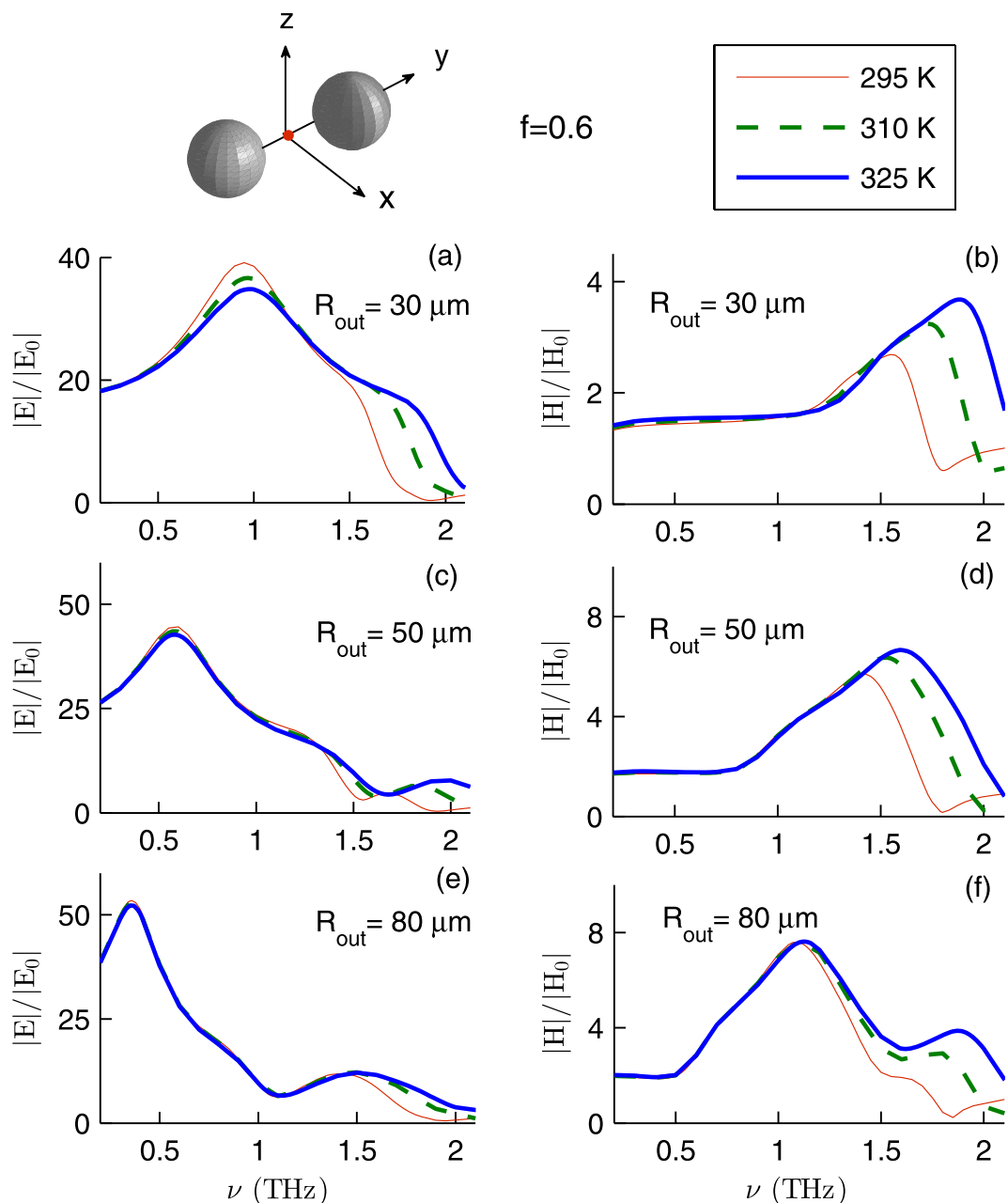


**Figure 4.** The field enhancement factors for InSb dimer as a function of  $\nu$  for various  $R_{\text{out}}$  and  $T$ . Here  $f=0.6$ ,  $\mathbf{E}_i \parallel \hat{\mathbf{y}}$ ,  $\mathbf{k}_i = -k\hat{\mathbf{z}}$ , and the fields are calculated at  $(\mathbf{r}_1 + \mathbf{r}_2)/2$ .

Figure 2 shows the enhancement factors of InSb dimer. Here  $T=295\text{ K}$ ,  $\mathbf{E}_i \parallel \hat{\mathbf{y}}$ , that is, the incident electric field is parallel with the dimer axis,  $\mathbf{k}_i = -k\hat{\mathbf{z}}$ , and the fields are calculated at the dimer center  $(\mathbf{r}_1 + \mathbf{r}_2)/2$ . Quite remarkably,  $|E/E_0|$  as large as (45.35, 47.36, 53.67) at frequency  $\nu_E = (0.85, 0.57, 0.36)$  THz is achievable with spheres of outer radius (30, 50, 80)  $\mu\text{m}$  and core fraction (0.8, 0.8, 0). Moreover,  $|H/H_0|$  as large as (3.15, 6.70, 7.85) at frequency  $\nu_H = (1.70, 1.51, 1.10)$  THz is achievable with spheres of outer radius (30, 50, 80)  $\mu\text{m}$  and core fraction (0, 0 and 0.2, 0 and 0.2). In the case of 30  $\mu\text{m}$  radius spheres,  $\nu_E$  slightly depends on  $f$ . Indeed  $\nu_E$  shifts from 1.0 to 0.85 THz as  $f$  increases from 0 to 0.8. However, for 50 and 80  $\mu\text{m}$  radius spheres,  $\nu_E$  does not depend on  $f$ . On the other hand  $\nu_H$  shows a more clear dependence on  $f$ . For 50  $\mu\text{m}$  radius spheres,  $\nu_H$  shifts from 1.51 to 1.25 THz as  $f$  increases from 0 to 0.8. Note that to obtain the largest enhancement at a certain frequency, the outer radius and core fraction must be chosen deliberately. For example at frequency 1.5 THz, 50  $\mu\text{m}$  spheres of core fraction 0.4 are superior to those of core fraction 0.8. At frequency 1 THz, 30  $\mu\text{m}$  radius spheres are superior (inferior) to 80  $\mu\text{m}$  radius ones in enhancing the electric (magnetic) field.

The *polarization* of the incident wave has a profound effect on the dimer optical response: The enhancement factors at the dimer center are not considerable when the incident electric field is perpendicular to the dimer axis.

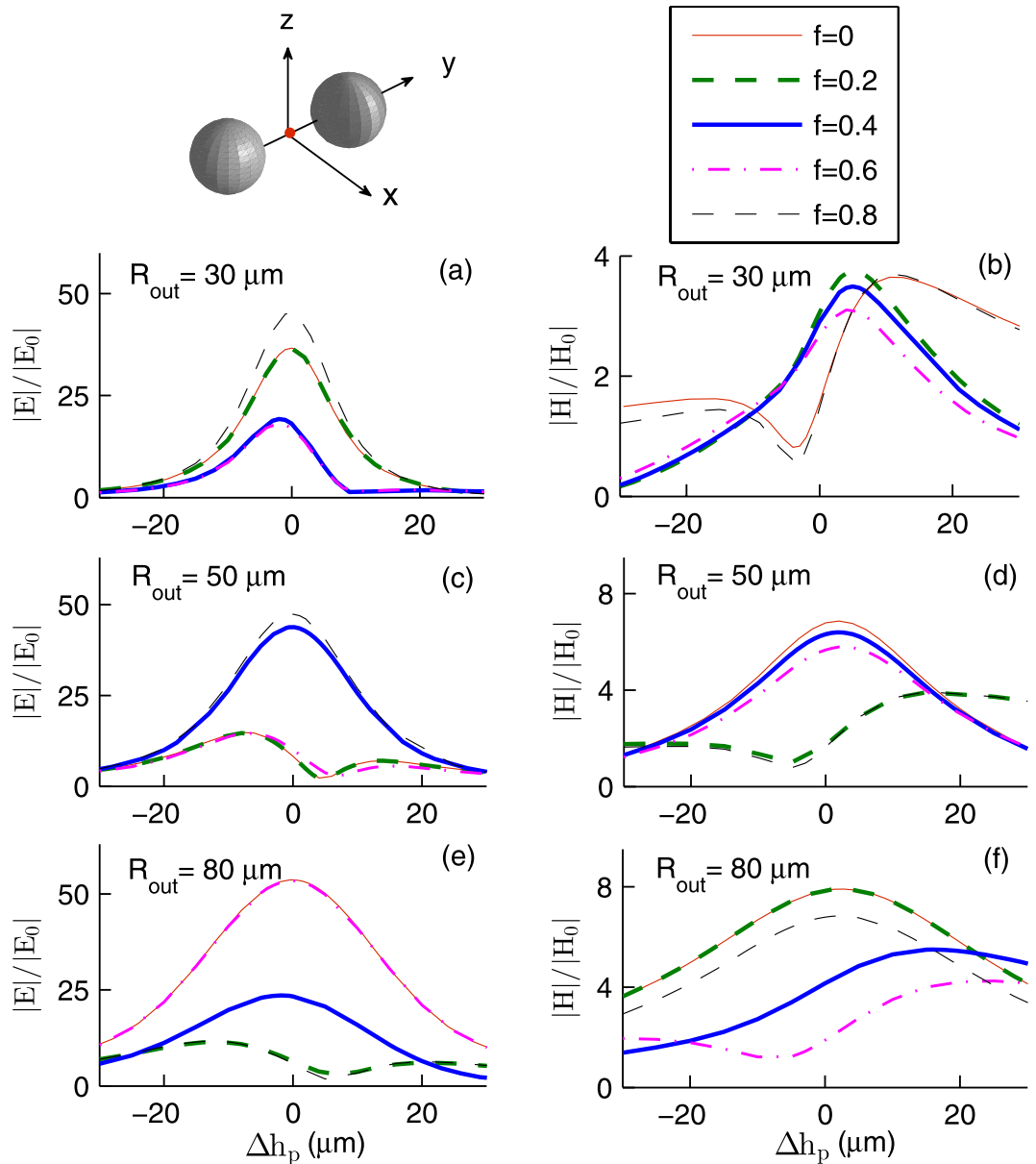


**Figure 5.** The field enhancements at the point  $(\mathbf{r}_1 + \mathbf{r}_2)/2 + \Delta h_p \hat{z}$  as a function of  $\Delta h_p$ . Here  $T = 295$  K,  $\mathbf{E}_I \parallel \hat{y}$ , and  $\mathbf{k}_I = -k\hat{z}$ . When  $f = (0, 0.2, 0.4, 0.6, 0.8)$  the frequency in THz is (a) (1.0, 0.99, 1.63, 1.55, 0.85), (b) (1.0, 1.67, 1.63, 1.55, 0.85), (c) (1.51, 1.51, 0.59, 1.41, 0.57), (d) (1.51, 0.59, 1.49, 1.41, 0.57), (e) (0.36, 1.1, 0.7, 0.36, 1.03), and (f) (1.1, 1.1, 0.7, 0.36, 1.03).

Now we pay attention to the symmetric trimer shown in Fig. 1. We assume that identical hollow microspheres are at  $\mathbf{r}_1$ ,  $\mathbf{r}_2$ , and  $\mathbf{r}_3 = (\sqrt{3}R_{out} + \sqrt{3}d_p/2, 0, h_p)$ . As before we assume that  $d_p = 2 \mu\text{m}$  and  $h_p = 1$  nm. Figure 3 shows the enhancement factors of InSb trimers. Here  $T = 295$  K,  $\mathbf{E}_I \parallel \hat{y}$ ,  $\mathbf{k}_I = -k\hat{z}$ , and the fields are calculated at  $(\mathbf{r}_1 + \mathbf{r}_2)/2$ . At first glance, Fig. 3 is not qualitatively different from Fig. 2. But upon a closer inspection, it becomes evident that the trimer may be used to *fine tune* the frequencies  $\nu_E$  and  $\nu_H$ . Here  $|E/E_0|$  as large as (34.73, 35.38, 39.37) at frequency  $\nu_E = (0.83, 0.55, 0.34)$  THz is possible with spheres of outer radius (30, 50, 80)  $\mu\text{m}$  and core fraction (0.8, 0.8, 0). Moreover,  $|H/H_0|$  as large as (3.04, 6.02, 7.21) at frequency  $\nu_H = (1.65, 1.49, 1.09)$  THz is possible with spheres of outer radius (30, 50, 80)  $\mu\text{m}$  and core fraction (0, 0 and 0.2, 0 and 0.2). In the case of 80  $\mu\text{m}$  radius spheres, the right shoulder of  $|E/E_0|$  is also of use. Here  $|E/E_0| = (17.12, 17.13, 16.90, 15.70, 12.76)$  at frequency (1.46, 1.47, 1.47, 1.43, 1.31) THz when  $f = (0, 0.2, 0.4, 0.6, 0.8)$ . Note that in a certain frequency window, the trimer may better act than the dimer. For example in the case of 80  $\mu\text{m}$  radius spheres of core fraction 0.8, the trimer better enhances the electric (magnetic) field in the frequency window 1.10–2 THz (1.44–2 THz).

We have also studied the field enhancement at the centroid of the trimer, assuming that  $T = 295$  K,  $\mathbf{E}_I \parallel \hat{x}$  or  $\mathbf{E}_I \parallel \hat{y}$ , and  $\mathbf{k}_I = -k\hat{z}$ . We find that the electric (magnetic) field at  $(\mathbf{r}_1 + \mathbf{r}_2 + \mathbf{r}_3)/3$  is about a factor ten (three) weaker than that at  $(\mathbf{r}_1 + \mathbf{r}_2)/2$ . Indeed with spheres of outer radius (30, 50, 80)  $\mu\text{m}$  and core fraction (0.8, 0.8, all values of  $f$ ), the maximum electric field enhancement (4.65, 3.63, 3.13) occurs at frequency  $\nu_E = (0.83, 0.55,$

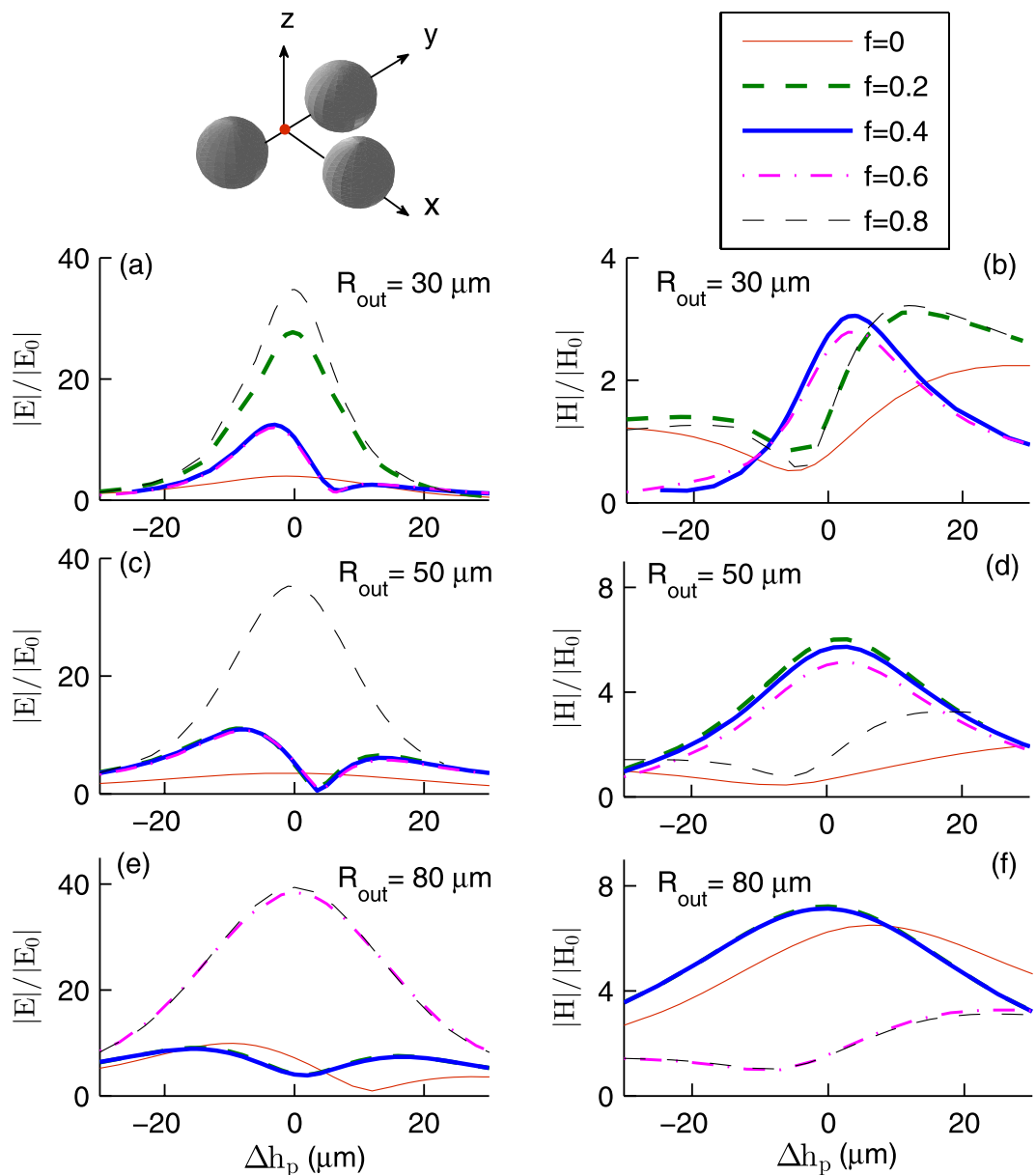


**Figure 6.** The field enhancements at the point  $(\mathbf{r}_1 + \mathbf{r}_2)/2 + \Delta h_p \hat{\mathbf{z}}$  as a function of  $\Delta h_p$ . Here  $T = 295$  K,  $\mathbf{E}_i \parallel \hat{\mathbf{y}}$ , and  $\mathbf{k}_i = -k\hat{\mathbf{z}}$ . When  $f = (0, 0.2, 0.4, 0.6, 0.8)$  the frequency in THz is (a and b) (1.87, 0.97, 1.61, 1.53, 0.83), (c and d) (1.85, 1.47, 1.45, 1.4, 0.55), (e and f) (0.95, 1.1, 1.1, 0.35, 0.33).

0.33) THz. With spheres of outer radius (30, 50, 80)  $\mu\text{m}$  and core fraction (0, 0, all values of  $f$ ), the maximum magnetic field enhancement (1.55, 2.25, 2.19) occurs at frequency  $\nu_H = (1.63, 1.45, 1.10)$  THz.

**The influence of ambient temperature on the field enhancement.** The plasma frequency  $\omega_p$  and the damping factor  $\gamma$  of InSb depend on the ambient temperature  $T$ . Naturally, the ambient temperature influences the hotspots provided by InSb microspheres. Figure 4 exemplifies the enhancement factors for InSb dimer for three different temperatures 295, 310 and 325 K. Here  $f = 0.6$ ,  $\mathbf{E}_i \parallel \hat{\mathbf{y}}$ ,  $\mathbf{k}_i = -k\hat{\mathbf{z}}$ , and the fields are calculated at  $(\mathbf{r}_1 + \mathbf{r}_2)/2$ . We find that the electric and magnetic field enhancement factors of (30, 50, 80)  $\mu\text{m}$  radius spheres show no clear temperature-dependence for frequencies lower than (0.50, 1.30, 1.49) THz and (1.20, 1.40, 1.10) THz, respectively. In the frequency window 1.5–2 THz, the enhancement factors increase as the temperature increases. For example, at frequency 1.80 THz the magnetic field enhancement of 50  $\mu\text{m}$  radius spheres increases from 0.16 to 5.15 as temperature increases from 295 to 325 K.

**The constructive interference of waves at the heart of the hotspots.** At first thought, one may expect the maximum field enhancement to occur at the center of symmetry  $\mathbf{r}_{\text{sym}}$  of a dimer or an equilateral trimer composed of similar microspheres. But the total field at a certain observation point  $\mathbf{r}_{\text{obs}}$  is due to the *interference* of the incident field and the fields scattered by the microspheres. The InSb permittivity and hence the Mie

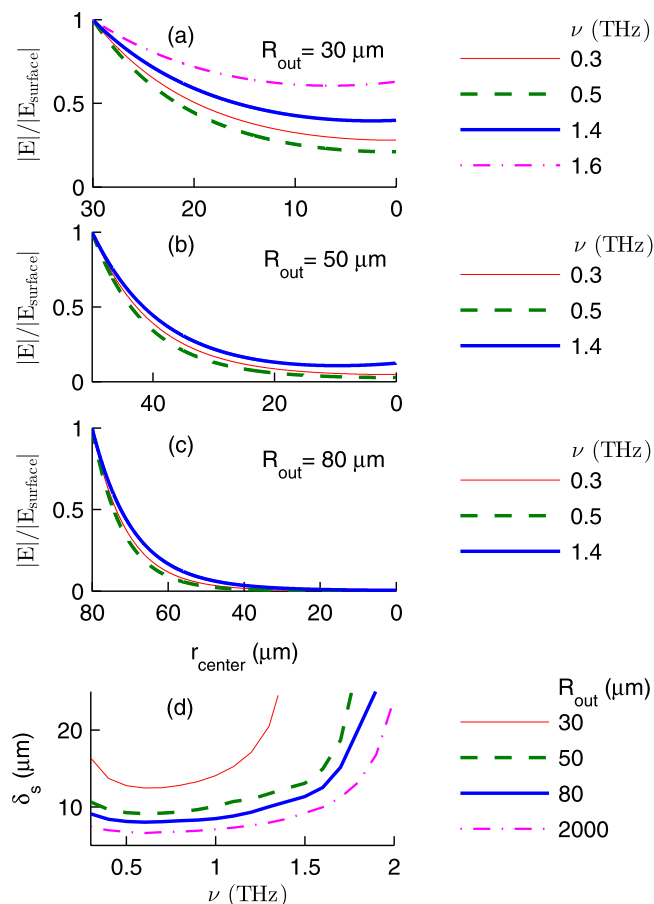


**Figure 7.** (a–c)  $|E/E_{\text{surface}}|$  of a solid InSb microsphere as a function of  $r_{\text{center}}$  for various outer radii and frequencies. (d) The skin depth  $\delta_s$  as a function of frequency  $\nu$  for various outer radii. Here  $T = 295 \text{ K}$ .

scattering coefficients depend on the frequency of the incident field. Thus the multipole fields induced in the microspheres depend on the frequency and polarization of the driving field. For a certain frequency and polarization, the incident and the scattered fields may interfere more constructively at  $\mathbf{r}_{\text{obs}}$  rather than at  $\mathbf{r}_{\text{sym}}$ . To confirm this, Figs 5 and 6 present field enhancements at a point displaced by the vector  $\Delta h_p \hat{\mathbf{z}}$  from the center of symmetry  $\mathbf{r}_{\text{sym}}$ . In many instances, the field reaches its maximum value when  $\Delta h_p \neq 0$ . Here for specified parameters  $\nu, f, R_{\text{out}}$ , etc., the maximum electric (magnetic) field enhancement occurs at a point below (above) the center of symmetry. For example, in the case of solid  $30 \mu\text{m}$  radius spheres subject to 1.0 THz (1.87 THz) radiation,  $|H/H_0|$  increases from 1.56 (0.78) to 3.65 (2.22) upon increasing the displacement from the center of the dimer (trimer) from zero to  $10.5 \mu\text{m}$  ( $25 \mu\text{m}$ ).

**The influence of core volume fraction on the field enhancements: The role of skin depth.** As a first approximation, each microsphere can be modeled as a pair of an electric dipole and a magnetic dipole. The total electric (magnetic) field acting on a microsphere and the electric polarizability (magnetic polarizability) determine the induced electric (magnetic) dipole. Both electric and magnetic polarizabilities depend on the inner and outer radii of the microsphere. Thus one expects the field enhancement factors to depend on the core volume fraction of the InSb microspheres. The generalized multiparticle Mie theory also confirms this<sup>30</sup>. However, Figs 2–4 show that  $|E/E_0|$  and  $|H/H_0|$  weakly depend on  $f$  in the frequency window 0.35–1.50 THz. This can be understood if one reminds that the skin depth  $\delta_s$ , the distance over which the electromagnetic wave penetrates into the material, depends on the frequency  $\nu$ .

Let us consider *one* solid InSb microsphere, and denote the radial distance from its centre, and the magnitude of the electric field at its surface by  $r_{\text{center}}$  and  $|E_{\text{surface}}|$ , respectively. Figure 7(a–c) demonstrate that for various outer radii and frequencies,  $|E/E_{\text{surface}}|$  is a *monotonically* decreasing function of  $r_{\text{center}}$ . Thus it is appropriate to introduce the skin depth  $\delta_s$  where  $|E/E_{\text{surface}}|$  is  $1/e \approx 0.368$ . Figure 7(d) shows extracted  $\delta_s$  as a function of  $\nu$  for various  $R_{\text{out}}$ . For example, in the case of  $80 \mu\text{m}$  radius spheres, the skin depth is  $8.46 \mu\text{m}$  at 1.0 THz. Thus we anticipate that at frequency 1.0 THz, the optical response of solid and hollow microspheres with  $R_{\text{in}} < 71.54 \mu\text{m}$  ( $f < 0.72$ ) are almost the same. The skin depth increases from  $11.33$  to  $25.55 \mu\text{m}$  as frequency increases from 1.5 to 2.0 THz. Hence we anticipate that in the frequency window 1.5–2.0 THz, the core fraction strongly influences the enhancement factors. Our detailed calculations are in agreement with these anticipations (see Figs 2–4). Figure 7(d) also shows that the skin depths for 80 and  $2000 \mu\text{m}$  radius spheres are not much different. Now it is clear that using large InSb microspheres, one finds that  $\nu_E$  and  $\nu_H$  very weakly depend on  $f$ . The skin depth of a

30  $\mu\text{m}$  radius sphere needs a separate discussion: Fig. 7(a) shows  $|E/E_{\text{surface}}|$  at frequencies 1.4 and 1.6 THz. Indeed  $\delta_s$  is not well defined for  $\nu > 1.35$  THz where  $|E/E_{\text{surface}}| > 0.368$  at  $r_{\text{center}} = 0$ .

## Conclusions

A few remarks are in order. (i) Here we have considered microspheres at a gap of 2  $\mu\text{m}$ . We expect the enhancement factors  $|E/E_0|$  and  $|H/H_0|$  to increase as the gap decreases. (ii) Here we have considered dimers and trimers of identical microspheres. Microspheres of different outer radius, core volume fraction, distance, and composition may allow better field enhancement. (iii) Populous disordered and fractal clusters of InSb microspheres deserve a separate study. (iv) It is instructive to remind the maximum enhancement factors in the wavelength window 400–1100 nm that dimers and trimers of hollow nanoparticles provide. Ag particles of outer radius 80 nm and core volume fraction 0.8 at a gap of 10 nm, provide electric field intensity enhancement as large as 2538 at wavelength 1020 nm. Using Si particles of outer radius 120 nm and core volume fraction 0.4 at a gap of 10 nm, magnetic field intensity enhancement as large as 109 at wavelength 612 nm is achievable<sup>30</sup>. Our results show that the field enhancements of InSb microspheres in the THz region of the spectrum are comparable to those of Ag and Si nanoparticles in the visible and near-infrared regions of the spectrum. (v) As early as 1978, Chen and Furdyna<sup>50</sup> prepared InSb microspheres by ultrasonically cutting small cylinders from a slab and abrading them in an air grinder. Recent successful fabrication of hollow InP microspheres<sup>51–53</sup> suggests that facile and cheap preparation of hollow InSb microspheres is not out of reach. (vi) The *simplicity* of using InSb microspheres to obtain reasonable THz electric and magnetic field enhancement, can be considered as an advantage.

In summary, we have studied electric and magnetic hotspots in the gap between hollow InSb microspheres forming dimers and trimers. To achieve field enhancement at a certain frequency corresponding to transition between energy levels of a molecule placed in the gap, the outer radius, core volume fraction, distance, and temperature of the microspheres can be chosen. For example, at the center of a dimer composed of 80  $\mu\text{m}$  radius spheres at a gap of 2  $\mu\text{m}$ , electric field intensity enhancements of 10–2880 and magnetic field intensity enhancements of 3–61 in the frequency window 0.35–1.50 THz are achievable. Here the incident electric field is parallel with the dimer axis, and  $T = 295$  K. The core volume fraction ( $0 \leq f \leq 0.8$ ) and the ambient temperature ( $295 \leq T \leq 325$  K) influence the intensity enhancements, particularly in the frequency window 1.5–2 THz. The enhancement factors are not considerable when the incident electric field is perpendicular to the dimer axis. Provided that all microspheres are fabricated with the same size, the maximum field enhancements presented by the trimer are less than those of the dimer. Nevertheless, in a certain frequency window, the trimer may be superior to the dimer. For instance using 80  $\mu\text{m}$  radius spheres of core fraction 0.2, the trimer better enhances the electric (magnetic) field in the frequency window 1.23–1.73 THz (1.59–1.75 THz). We have shown that the frequency dependence of the skin depth explains the weak dependence of the enhancement factors on the core volume fraction. Electric and magnetic hotspots provided by InSb microspheres are promising for THz absorption and circular dichroism spectroscopy.

## References

- Lee, Y.-S. *Principles of Terahertz Science and Technology*. (Springer, New York, 2009).
- Zhang, X.-C. & Xu, J. *Introduction to THz Wave Photonics*. (Springer, New York, 2010).
- Schmuttenmaer, C. A. Exploring dynamics in the far-infrared with terahertz spectroscopy. *Chem. Rev.* **104**, 1759–1779 (2004).
- Fumino, K., Reimann, S. & Ludwing, R. Probing molecular interaction in ionic liquids by low frequency spectroscopy: coulomb energy, hydrogen bonding and dispersion forces. *Phys. Chem. Chem. Phys.* **16**, 21903–21929 (2014).
- Heugen, U. *et al.* Solute-induced retardation of water dynamics probed directly by terahertz spectroscopy. *Proc. Natl. Acad. Sci. USA* **103**, 12301–12306 (2006).
- Markelz, A., Whitmire, S., Hillebrecht, J. & Birge, R. THz time domain spectroscopy of biomolecular conformational modes. *Phys. Med. Biol.* **47**, 3797–3805 (2002).
- Kumar, S. *et al.* Terahertz spectroscopy of single-walled carbon nanotubes in a polymer film: observation of low-frequency phonons. *J. Phys. Chem. C* **114**, 12446–12450 (2010).
- Harde, H., Cheville, R. A. & Grischkowsky, D. Collision-induced tunneling in methyl halides. *J. Opt. Soc. Am. B.* **14**, 3282–3293 (1997).
- Xu, J. *et al.* Terahertz circular dichroism spectroscopy: a potential approach to the *in situ* detection of life's metabolic and genetic machinery. *Astrobiology* **3**, 489–504 (2003).
- Choi, J.-H. & Cho, M. Terahertz chiroptical spectroscopy of an  $\alpha$ -helical polypeptide: a molecular dynamics simulation study. *J. Phys. Chem. B.* **118**, 12837–12843 (2014).
- Jenkins, G. S., Schmadel, D. C. & Drew, H. D. Simultaneous measurement of circular dichroism and Faraday rotation at terahertz frequencies utilizing electric field sensitive detection via polarization modulation. *Rev. Sci. Instrum.* **81**, 083903 (2010).
- Wei, H. & Xu, H. Hot spots in different metal nanostructures for plasmon-enhanced Raman spectroscopy. *Nanoscale* **5**, 10794–10805 (2013).
- Adato, R., Aksu, S. & Altug, H. Engineering mid-infrared nanoantennas for surface enhanced infrared absorption spectroscopy. *Mater. Today* **18**, 436–446 (2015).
- Neubrech, F., Huck, C., Weber, K., Pucci, A. & Giessen, H. Surface-enhanced infrared spectroscopy using resonant nanoantennas. *Chem. Rev.* **117**, 5510–5145 (2017).
- Bek, A. *et al.* Fluorescence enhancement in hot spots of AFM-designed gold nanoparticle sandwiches. *Nano Lett.* **8**, 485–490 (2008).
- Gill, R. & Le., Ru, E. C. Fluorescence enhancement at hot-spots: the case of Ag nanoparticle aggregates. *Phys. Chem. Chem. Phys.* **13**, 16366–16372 (2011).
- Punj, D. *et al.* Self-assembled nanoparticle dimer antennas for plasmonic-enhanced single-molecule fluorescence detection at micromolar concentrations. *ACS Photonics* **2**, 1099–1107 (2015).
- Abdali, S. & Blanch, E. W. Surface enhanced Raman optical activity (SEROA). *Chem. Soc. Rev.* **37**, 980–992 (2008).
- Wang, H., Li, Z., Zhang, H., Wang, P. & Wen, S. Giant local circular dichroism within an asymmetric plasmonic nanoparticle trimer. *Sci. Rep.* **5**, 8207 (2015).
- Albella, P., Alcaraz de la Osa, R., Moreno, F. & Maier, S. A. Electric and magnetic field enhancement with ultralow heat radiation dielectric nanoantennas: considerations for surface-enhanced spectroscopies. *ACS Photonics* **1**, 524–529 (2014).
- Caldarola, M. *et al.* Non-plasmonic nanoantennas for surface enhanced spectroscopies with ultra-low heat conversion. *Nat. Commun.* **6**, 7915 (2015).

22. Albella, P. *et al.* Low-loss electric and magnetic field-enhanced spectroscopy with subwavelength silicon dimers. *J. Phys. Chem. C* **117**, 13573–13584 (2013).
23. Bakker, R. M. *et al.* Magnetic and electric hotspots with silicon nanodimers. *Nano Lett.* **15**, 2137–2142 (2015).
24. Boudarham, G., Abdeddaim, R. & Bonod, N. Enhancing the magnetic field intensity with a dielectric gap antenna. *Appl. Phys. Lett.* **104**, 021117 (2014).
25. Craig, D. P. & Thirunamachandran, T. *Molecular Quantum Electrodynamics*. (Academic Press, New York, 1984).
26. García-Etxarri, A. & Dionne, J. A. Surface-enhanced circular dichroism spectroscopy mediated by nonchiral nanoantennas. *Phys. Rev. B* **87**, 235409 (2013).
27. Ho, C. S., García-Etxarri, A., Zhao, Y. & Dionne, J. A. Enhancing enantioselective absorption using dielectric nanospheres. *ACS Photonics* **4**, 197–203 (2017).
28. Sheikholeslami, S. N., García-Etxarri, A. & Dionne, J. A. Controlling the interplay of electric and magnetic modes via Fano-like plasmon resonances. *Nano Lett.* **11**, 3927–3934 (2011).
29. Alegret, J. *et al.* Plasmonic properties of silver trimers with trigonal symmetry fabricated by electron-beam lithography. *J. Phys. Chem. C* **112**, 14313–14317 (2008).
30. Miri, M. F. & Sadra, M. Dimers and trimers of hollow silicon nanoparticles: manipulating the magnetic hotspots. *J. Phys. Chem. C* **121**, 11672–11679 (2017).
31. Stockman, M. I., Pandey, L. N. & George, T. F. Inhomogeneous localization of polar eigenmodes in fractals. *Phys. Rev. B* **53**, 2183–2186 (1996).
32. Stockman, M. I. Inhomogeneous eigenmode localization, chaos, and correlations in large disordered clusters. *Phys. Rev. E* **56**, 6494–6507 (1997).
33. Bozhevolnyi, S. I., Markel, V. A., Coello, V., Kim, W. & Shalaev, V. M. Direct observation of localized dipolar excitations on rough nanostructured surfaces. *Phys. Rev. B* **58**, 11441–11448 (1998).
34. Markel, V. A. *et al.* Near-field optical spectroscopy of individual surface-plasmon modes in colloid clusters. *Phys. Rev. B* **59**, 10903–10909 (1999).
35. Naeimi, Z. & Miri, M. F. Magnetic and electric hotspots via fractal clusters of hollow silicon nanoparticles. *Opt. Lett.* **43**, 462–465 (2018).
36. Koo, S., Kumar, M. S., Shin, J., Kim, D. & Park, N. Extraordinary magnetic field enhancement with metallic nanowire: role of surface impedance in Babinet's principle for sub-skin-depth regime. *Phys. Rev. Lett.* **103**, 263901 (2009).
37. Giannini, V., Berrier, A., Maier, S. A., Sánchez-Gill, J. A. & Rivas, J. G. Scattering efficiency and near field enhancement of active semiconductor plasmonic antennas at terahertz frequencies. *Opt. Express* **18**, 2797–2807 (2010).
38. Park, H.-R. *et al.* Colossal absorption of molecules inside single terahertz nanoantennas. *Nano Lett.* **13**, 1782–1786 (2013).
39. Feuillet-Palma, C., Todorov, Y., Vasaneli, A. & Sirtori, C. Strong near field enhancement in THz nano-antenna arrays. *Sci. Rep.* **3**, 1361 (2013).
40. Toma, A. *et al.* Squeezing terahertz light into nanovolumes: nanoantenna enhanced terahertz spectroscopy (NETS) of semiconductor quantum dots. *Nano Lett.* **15**, 386–391 (2014).
41. Zhang, Y. & Han, Z. Spoof surface plasmon based planar antennas for the realization of terahertz hotspots. *Sci. Rep.* **5**, 18606 (2015).
42. Klarskov, P., Tarekge, A. T., Iwaszczuk, K., Zhang, X.-C. & Jepsen, P. Amplification of resonant field enhancement by plasmonic lattice coupling in metallic slit arrays. *Sci. Rep.* **6**, 37738 (2016).
43. Savoini, M. *et al.* THz near-field enhancement by means of isolated dipolar antennas: the effect of finite sample size. *Opt. Express* **24**, 4552–4562 (2016).
44. Hanham, S. M. *et al.* Broadband terahertz plasmonic response of touching InSb disks. *Adv. Mater.* **24**, OP226–OP230 (2012).
45. Rivas, J. G., Kuttge, M., Kurz, H., Bolivar, P. H. & Sánchez-Gil, J. A. Low-frequency active surface plasmon optics on semiconductors. *Appl. Phys. Lett.* **88**, 082106 (2006).
46. Fan, F., Chen, S. & Chang, S. J. A review of magneto-optical microstructure devices at terahertz frequencies. *IEEE J. Sel. Top. Quantum Electron.* **23**, 1–12 (2017).
47. Howells, S. C. & Schlie, L. A. Transient terahertz reflection spectroscopy of undoped InSb from 0.1 to 1.1 THz. *Appl. Phys. Lett.* **69**, 550–552 (1996).
48. Oszwaldowski, M. & Zimpel, M. Temperature dependence of intrinsic carrier concentration and density of states effective mass of heavy holes in InSb. *J. Phys. Chem. Solids* **49**, 1179–1185 (1988).
49. Sánchez-Gil, J. A. & Gómez Rivas, J. Thermal switching of the scattering coefficients of terahertz surface plasmon polaritons impinging on a finite array of subwavelength grooves on semiconductor surfaces. *Phys. Rev. B* **73**, 205410 (2006).
50. Chen, K. K. & Furdyna, J. K. Microwave propagation in InSb powder: magnetoplasma and heliconwave excitations. *J. Appl. Phys.* **46**, 3363–3377 (1978).
51. Zheng, X., Liu, C. & Xie, Y. An analogous solution-liquid-solid (ASLS) growth route to InP hollow spheres and a honeycomb-like macroporous framework. *Eur. J. Inorg. Chem.* **12**, 2364–2369 (2006).
52. Zheng, X., Hu, Q. & Sun, C. Efficient rapid microwave-assisted route to synthesize InP micrometer hollow spheres. *Mater. Res. Bull.* **44**, 216–219 (2009).
53. Bao, K., Sun, H., Zhu, L. & Cao, J. Synthesis of InP hierarchical microspheres and its optical property. *Sens. Actuators B* **150**, 649–654 (2010).

## Acknowledgements

We thank the financial support from the Iran National Science Foundation (INSF), research Grant No. 96008207.

## Author Contributions

The idea of the study was conceived by M.F.M. M.S. carried out the numerical simulations. All authors contributed to the scientific discussion and wrote the paper.

## Additional Information

**Competing Interests:** The authors declare no competing interests.

**Publisher's note:** Springer Nature remains neutral with regard to jurisdictional claims in published maps and institutional affiliations.



**Open Access** This article is licensed under a Creative Commons Attribution 4.0 International License, which permits use, sharing, adaptation, distribution and reproduction in any medium or format, as long as you give appropriate credit to the original author(s) and the source, provide a link to the Creative Commons license, and indicate if changes were made. The images or other third party material in this article are included in the article's Creative Commons license, unless indicated otherwise in a credit line to the material. If material is not included in the article's Creative Commons license and your intended use is not permitted by statutory regulation or exceeds the permitted use, you will need to obtain permission directly from the copyright holder. To view a copy of this license, visit <http://creativecommons.org/licenses/by/4.0/>.

© The Author(s) 2019